Optically Sampled Analog-to-Digital Converters

Paul W. Juodawlkis, *Member, IEEE*, Jonathan C. Twichell, *Member, IEEE*, Gary E. Betts, *Member, IEEE*, Jeffrey J. Hargreaves, *Member, IEEE*, Richard D. Younger, Jeffrey L. Wasserman, *Member, IEEE*, Fredrick J. O'Donnell, Kevin G. Ray, and Richard C. Williamson, *Fellow, IEEE*

Invited Paper

***Abstract*—Optically sampled analog-to-digital converters (ADCs) combine optical sampling with electronic quantization to enhance the performance of electronic ADCs. In this paper, we review the prior and current work in this field, and then describe our efforts to develop and extend the bandwidth of a linearized sampling technique referred to as phase-encoded optical sampling. The technique uses a dual-output electrooptic sampling transducer to achieve both high linearity and 60-dB suppression of laser amplitude noise. The bandwidth of the technique is extended by optically distributing the post-sampling pulses to an array of time-interleaved electronic quantizers. We report on the performance of a 505-MS/s (megasample per second) optically sampled ADC that includes high-extinction $LiNbO_3$ 1-to-8 optical time-division demultiplexers. Initial characterization of the 505-MS/s system reveals a maximum signal-to-noise ratio of 51 dB (8.2 bits) and a spur-free dynamic range of 61 dB. The performance of the present system is limited by electronic quantizer noise, photodiode saturation, and preliminary calibration procedures. None of these fundamentally limit this sampling approach, which should enable multigigahertz converters with 12-b resolution. A signal-to-noise analysis of the phase-encoded sampling technique shows good agreement with measured data from the 505-MS/s system.**

***Index Terms*—Analog–digital conversion, distortion, electrooptic devices, intermodulation, microwave receivers, pulsed lasers, signal sampling, time-division multiplexing.**

I. Introduction

ADVANCED radar, surveillance, and communication systems could benefit significantly from high-resolution (12+ bits) analog-to-digital converters (ADCs) having mutligigahertz of instantaneous bandwidth. The flexibility of the receivers in these systems can be augmented by pushing the ADC closer to the antenna and performing more of the receiver functions (i.e., out-of-band rejection, down conversion, matched filtering, detection) in the digital domain. The ability to implement these digital-receiver architectures is often limited by the performance of the ADC component. For example, electronic ADCs with sampling rates >1 GS/s (gigasample per second) are presently limited to resolutions of less than seven effective bits [44-dB signal-to-noise ratio (SNR)] [1], and ADCs having 12 effective bits (74-dB SNR) have a maximum sampling rate of 65 MS/s (megasample per second) [2]. Additionally, the rate-of-improvement of high-speed ADCs is substantially slower than that of digital signal-processing (DSP) hardware. Over a recent eight-year period, the average increase in ADC resolution for a given sampling rate was only 1.5 bits [1].

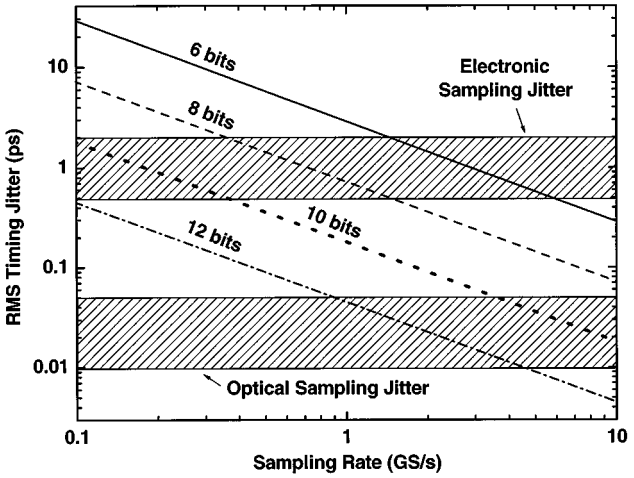

Fig. 1. Timing-jitter requirement for ADCs as a function of sampling rate and number of effective bits. The calculation assumes that timing jitter is the only noise source. The present-day electronic and optical sampling-aperture jitter ranges (hatched areas) are from [1], [10], and [11].

In addition to the inherent quantization noise, the resolution of electronic ADCs is limited by a number of mechanisms including thermal noise, sampling aperture jitter, and comparator ambiguity [1]. Thermal noise appears to dominate the performance of high-resolution low-bandwidth ADCs while aperture jitter and comparator ambiguity become important at high sampling rates. Fig. 1 illustrates the allowable timing jitter for a Nyquist ADC (i.e., maximum input frequency = 1/2 sampling rate) as a function of sampling rate and effective bits, assuming that jitter is the only error source. Estimates of aperture jitter in state-of-the-art electronic ADCs range from 0.5 to 2 ps (see hatched region in Fig. 1), indicating that electronic aperture jitter is presently a major limit to the performance of high-speed high-resolution ADCs. For example, the 50-fs timing jitter required to implement a 1-GS/s 12-bit converter is far below that of present electronic jitter estimates. In contrast, sampling-aperture jitter less than 50 fs has been attained in optical sampling systems, as discussed below.

Manuscript received January 17, 2001; revised May 25, 2001. This work was supported by the Defense Advanced Research Projects Agency Photonic A/D Converter Technology (PACT) Program under Air Force Contract F19628-00-C-0002.

The authors are with the Lincoln Laboratory, Massachusetts Institute of Technology, Lexington, MA 02420-9108 USA.

Publisher Item Identifier S 0018-9480(01)08727-0.

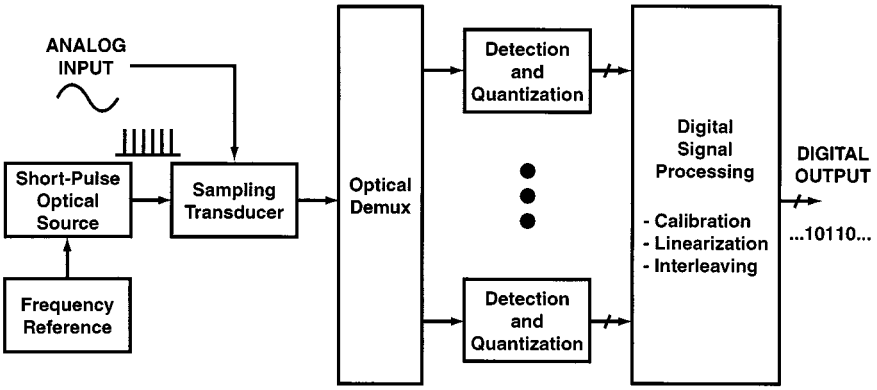

Fig. 2. Generic architecture of an optically sampled time-interleaved ADC.

ADCs with increased bandwidth can be realized by time interleaving the quantized samples from a parallel array of slower converters [3]. This time-interleaved approach has been used in a number of all-electronic ADCs [4]–[6]. The principle difficulty in implementing a time-interleaved ADC is making the interleaved samples from the slow-converter array appear as though they were generated by a single fast converter. Converter matching errors will produce spurs in the spectra of the time-interleaved ADC output samples. To achieve a large spur-free dynamic range (SFDR) in a time-interleaved ADC, the following conditions must be met.

1) The sampling times of the interleaved ADCs must be uniform [7].
2) The converter-to-converter gains and offsets must be precisely matched [3], [8].
3) The crosstalk between ADC converters and sample-to-sample memory effects must be minimal [9].

For example, to achieve an interleaving SFDR of 80 dB, the converter-to-converter gains must be matched to $\sim$0.01%, the offsets must be matched to $\sim$0.01% of the signal amplitude, and the converter-to-converter crosstalk must be less than one part in 10^4.

In this paper, we describe the use of optical sampling to extend the performance of electronic ADCs. In the approach presented here, the sampling function is performed in the optical domain and quantization is performed in the electronic domain (Fig. 2). The principal advantages of optical sampling are: 1) modern mode-locked lasers can produce high-frequency ($>$10 GHz) periodic sequences of optical pulses with timing jitter significantly below that of electronic circuitry, and 2) the sampling process can be made to be highly linear with negligible back-coupling between the optical sampling pulses and the electrical signal being sampled. The timing jitter of actively mode-locked fiber lasers has been measured to be $<$10 fs over narrow-band integration limits (100 Hz to 1 MHz) [10] and $<$50 fs pulse to pulse [11] (see hatched region in Fig. 1). These precisely timed optical clock pulses can be used to sample an electrical signal via a transducer that converts electrical signal variations into optical-pulse intensity or energy variations. Following the sampling transducer, the pulses are converted to electrical signals using photodetectors and quantized using electronic ADCs. The bandwidth of the optical sampling technique can be extended by distributing the post-sampling pulses to an array of time-interleaved electronic quantizers. Distribution can be achieved in the optical domain by using optical demultiplexers having low channel-to-channel crosstalk.

We begin the paper (Section II) with a survey of the past and present work in the field of photonic ADCs. Section III describes our phase-encoded optical sampling technique that provides both high linearity and large suppression of laser amplitude noise. We review our previous results on phase-encoded sampling and discuss calibration requirements and performance limitations. In Section IV, we present the initial characterization of a 505-MS/s optically sampled ADC that includes high-extinction $LiNbO_3$ 1-to-8 optical time-division demultiplexers. The SNR and SFDR of the current 505-MS/s photonic ADC are 51 and 61 dB, respectively. Factors limiting the performance of these initial results are discussed. An SNR analysis of the phase-encoded sampling technique is included in the Appendix. This analysis accounts for both shot noise and uncorrelated detection/quantization noise.

II. Survey of Optically Sampled ADCs

The use of short optical pulses to sample electrical signals has been investigated for a number of years [12], [13]. A proposal by Taylor [14], [15] that combined optical sampling with an opto-electronic quantization scheme led to the development of a photonic 1-GS/s 4-b ADC [16]. The quantization scheme was based on an array of electrooptic interferometers having half-wave voltages organized in a binary ladder. Although this architecture was limited in resolution, these results highlighted the benefits provided by the application of optical sampling to the front end of an ADC.

The concepts of optical sampling and time interleaving were first combined by Bell *et al.* to realize a 2-GS/s hybrid optical/electronic ADC that achieved a resolution of 2.8 effective bits (18.5-dB SNR) when undersampling a 10.3-GHz sinusoid [17], [18]. In this ADC, the optical pulse source was a laser diode that was gain switched using a 2-GHz step-recovery diode. The electrical input signal was sampled by passing the laser pulses through a single-output $LiNbO_3$ Mach–Zehnder

(MZ) interferometer having an 18-GHz bandwidth. Time interleaving was implemented by using an active 1-to-4 optical switch to distribute the interferometer output pulses to four parallel channels of detection electronics. Each detection channel consisted of a photodetector, a wide-band amplifier, and an ADC operating at 500 MS/s. This distribution approach can be regarded as 1-to-N time demultiplexing since a temporal window is created to route every Nth pulse (in this case, $N = 4$) to the same channel, thereby reducing the effective data rate into each electronic ADC by a factor of N. The authors of this paper concluded that the primary SNR limits were the pulse-to-pulse timing jitter ($\sim$1 ps) and intensity noise ($\sim$2.5%) of the gain-switched laser diode.

As an alternative to the optical time-division demultiplexing approach just described, wavelength-division demultiplexing has also been used in optically sampled time-interleaved ADCs. In these architectures, spectrally broad and temporally short optical pulses are either: 1) temporally broadened using a dispersive medium [19], [20] or 2) separated into N distinct pulses, each at a different wavelength, with interpulse temporal spacing of T/N, where T is the period of the initial pulse train [21]–[24]. Discrete-wavelength pulse separation has been achieved using a wavelength-division multiplexer (WDM) along with fiber delay lines [21], [23] and an arrayed-waveguide grating (AWG) with integrated feedback waveguides [22], [24]. These demonstrations have all utilized a single-output MZ to perform the sampling function. After sampling the signal, the single temporally broad pulse or N discrete pulses are routed to N parallel channels of detection electronics using a passive wavelength-division demultiplexer. This passive demultiplexing is an advantage of the wavelength-division technique relative to the time-division technique, which requires an active demultiplexer containing accurately timed optical switches. However, this advantage is attained at the expense of a significantly more complex optical source that must generate a periodically repeating mutliwavelength pulse train with very precise interpulse spacing. Continuous-sampling implementations of the wavelength-division approach have been demonstrated at 160 MS/s using a 1-to-4 demultiplexer [21] and 12-GS/s using a 1-to-3 demultiplexer [24]. The 12-GS/s (1-to-3) ADC achieved 2-b resolution (14-dB SNR) when sampling a 3.6-GHz signal [24], [25]. An estimated resolution of 7 bits (44-dB SNR) was obtained from a single 1.25-GS/s channel of a 10-GS/s (1-to-8) noncontinuous sampling demonstration [23]. The principal limit to the ADC resolution in both of these papers was attributed to laser noise.

The optical sampling architecture described above is only one method of applying optics to the ADC problem. The photonic time-stretch technique [26]–[28] involves increasing the time duration of a fast electrical signal so that it can be sampled using a slower ADC. The time-stretch function is performed by sampling an electrical signal with a chirped pulse and then temporally lengthening the pulse using a dispersive medium such as an optical fiber. Pulse-stretch factors of eight [27] and sampling rates of 30 GS/s have been demonstrated [28]. Optical sampling has also been performed using the photoconductive property of photodiodes [29], [30]. Other optical quantization schemes involving all-optical nonlinear devices [31]–[34], symmetric self-electrooptic effect devices (S-SEEDs) [35], opto-electronic comparators [36], distributed phase modulation [37], and diffractive optics [38] have been investigated. Photonic ADCs based on optical oversampling techniques, such as delta–sigma (Δ–Σ) architectures, have also been reported [39], [40].

III. Phase-Encoded Optical Sampling

A. Overview

In most of the optical sampling demonstrations described above, the sampling transducer was an $LiNbO_3$ electrooptic MZ interferometer having a single output. An electrical signal applied to the interferometer modulates the intensity and, hence, the energy, of a sequence of precisely timed optical pulses that are transmitted through the interferometer. The intensity of each output pulse has a direct correspondence to the applied voltage at the time the pulse traversed the modulator. Below, we refer to optical sampling using single-output interferometers as *intensity sampling*. The relationship between the MZ modulator optical transmission $T_{\rm MZ}$ and the applied voltage $V_{\rm IN}$ is accurately described by

$$T_{\rm MZ} = \frac{1}{2}\left(1 + C\sin\left(\frac{\pi \cdot V_{\rm IN}}{V_\pi} + \theta\right)\right) \tag{1}$$

where C is the modulator's contrast ratio ($C = 1$ corresponds to infinite on/off extinction), V_π is the modulator's half-wave voltage, and θ is a phase angle describing the interferometer's deviation from quadrature with $V_{\rm IN} = 0$. This relationship is appropriate for $LiNbO_3$ MZ modulators because: 1) the phase shift induced by the electrooptic effect is highly linear in applied field and 2) the ideal sinusoidal MZ phase-to-intensity conversion can be approached in $LiNbO_3$ integrated-optic interferometers. The dynamic range of photonic ADCs using MZ sampling transducers is limited by the sinusoidal nonlinearity in (1) unless linearization techniques are utilized.

A number of approaches to linearize the MZ interferometer transmission function have been reported. Optical linearization techniques involving multiple interferometers connected in series or parallel configurations have demonstrated SFDR performance close to theoretical limits, but often have limited bandwidth and are complex to implement [41], [42]. Work has also been done to modify the electrical signal before applying it to the modulator so that the limiting odd-order nonlinear terms are greatly suppressed [43], [44]. When the final output of the optical system is digital, as in the case of a photonic ADC, linearization can be performed computationally by direct inversion of the modulator transfer function of (1). Digital linearization has been demonstrated at modulation indexes $m = V_{\rm IN,\,P-P}/V_\pi$ as large as 0.83 where the third-order distortion was suppressed by 21 dB [45].

In our optical sampling architecture, we use a digital linearization technique referred to as *phase-encoded optical sampling* that combines the energy from the complementary outputs of a dual-output modulator to invert the MZ transfer function (Fig. 3) [46]. If a pulse of energy E_0 is transmitted through the

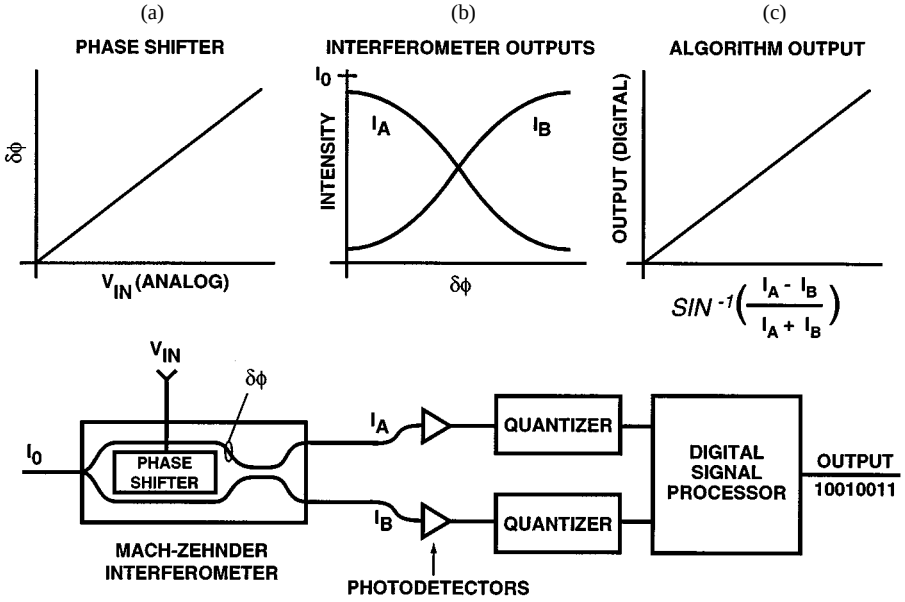

Fig. 3. Phase-encoded optical sampling technique. (a) Electrooptic effect provides a linear phase shift with respect to the applied voltage. (b) Complementary interferometer output intensities are sinusoidal with respect to the induced phase shift. (c) The phase shift and, therefore, the applied voltage is recovered by inverting the interferometer transfer function.

dual-output modulator at time t_0, the pulse energies at the output ports will be

$$E_A = \frac{E_0}{2}\left(1 + C\sin\left(\frac{\pi \cdot V_{\rm IN}(t_0)}{V_\pi} + \theta\right)\right) \tag{2}$$

$$E_B = \frac{E_0}{2}\left(1 - C\sin\left(\frac{\pi \cdot V_{\rm IN}(t_0)}{V_\pi} + \theta\right)\right) \tag{3}$$

where $V_{\rm IN}(t_0)$ is the voltage applied to the modulator at time t_0, and we assume that the sampling is instantaneous (i.e., negligible pulsewidth and time-of-propagation through the modulator). After measuring E_A and E_B, the applied voltage can be determined as

$$V_{\rm IN}(t_0) = \frac{V_\pi}{\pi}\left[\sin^{-1}\left(\frac{1}{C}\cdot\frac{E_A - E_B}{E_A + E_B}\right) - \theta\right]. \tag{4}$$

There are several points worth noting about this linearization method. First, the linearity is only limited by the accuracy to which E_A and E_B can be measured and to the extent that the modulator's transmission characteristic is represented by (1). If (4) is to be computed digitally, the linearity of E_A and E_B must be maintained though the photodetection, signal conditioning, and electronic quantization processes. Second, assuming perfect measurement of E_A and E_B, the estimate of $V_{\rm IN}(t_0)$ is independent of the input pulse energy E_0. This implies that the phase-encoded sampling technique is insensitive to laser amplitude noise. Indeed, the amplitude noise suppression of this technique has been measured to be at least 60 dB [11]. Third, small deviations of the modulator bias point from quadrature ($\theta \neq 0$) cause only a dc offset error and do not degrade the linearity, as in the case of the single-output digital linearization approach [45].

The primary tradeoff associated with the phase-encoded optical sampling technique is that it requires twice the number of well-calibrated electronic detection and quantization channels as the single-output intensity sampling technique.

B. Previous Results

The phase-encoded sampling technique was initially demonstrated by constructing a narrow-band UHF sampler that consisted of a 1.3-μm gain-switched laser diode, a dual-output $LiNbO_3$ MZ modulator, and a pair of InGaAs photodiodes followed by 12-b 1-MS/s quantizers [46]. The laser diode was gain switched via a 500-MHz step-recovery diode, producing 130-ps pulses with an estimated jitter of 1 ps. The outstanding linearity of the technique was verified by deliberately aliasing (down-converting) a pair of tones having frequencies near the laser repetition rate (i.e., 499.90 and 449.91 MHz) into the 500-kHz quantizer bandwidth. The two-tone third-order intermodulation (IM3)-free dynamic range was measured to be *greater than 90 dB* and was limited by the quantizer noise floor. This value of IM3 represented an improvement of at least 20 dB relative to intensity sampling at the same modulation depth.

The bandwidth of the phase-encoded sampling technique was later extended to 104 MHz by time interleaving an array of 12-b electronic quantizers (Analog Devices AD6640) operating at 52 MS/s [47]. The optical pulse source was a 1.55-μm harmonically mode-locked erbium-doped fiber laser producing 30-ps pulses at a 208-MS/s repetition rate. After sampling the electrical signal using a dual-output MZ modulator, the pulses were distributed to the eight parallel detection and quantization channels using a pair of 1-to-4 $LiNbO_3$ optical time-division demultiplexers. An integrate-and-reset detection circuit was used to reduce the required accuracy of the electronic quantizer sampling clock (see Section IV for details). The two-tone IM3 was measured to be 87 dB for $m = 0.15$, representing an improvement of 38 dB relative to that calculated for ideal intensity sampling, and demonstrating that linearity can be maintained in an optically

demultiplexed system. The overall system SFDR was limited to 65 dB by interleaving spurs that result from a combination of residual offset and gain errors, channel-to-channel crosstalk in the demultiplexers, and sample-to-sample memory effects in the detection circuits. Swept-frequency measurements (see crosstalk discussion below) revealed that a major error mechanism was the sample memory in the integrate-and-reset circuit. Potential causes of this memory include incomplete reset of the integration capacitor and photocurrent tails in the photodiodes. The SNR of the data set exhibiting the 65-dB SFDR was 47 dB (7.5 bits).

An analysis has been performed to quantify the relationship between the crosstalk mechanisms in a time-interleaved photonic ADC and the characteristics of the spurs associated with interleaving [9]. The two primary sources of crosstalk are channel-to-channel crosstalk in the demultiplexer and sample-to-sample memory effects in the detection circuitry. The analysis reveals that crosstalk introduces complex gain errors that result in frequency-dependent spurs when multiple channels are time interleaved. In general, the spur amplitudes are determined by a weighted sum of the different crosstalk terms over all channels in an interleaved ADC. For the simple case of crosstalk in only one channel of an N-channel ADC, the spur level relative to an input signal with frequency f_0 can be written as

$$\frac{P_{\mathrm{SPUR}}}{P_{\mathrm{SIGNAL}}} = 20\log\left[\frac{2\kappa|\sin(\pi f_0 \tau)|}{N}\right] \tag{5}$$

where κ is the magnitude of the crosstalk error and τ is delay between the desired pulse and the crosstalk pulse. This relation can be used to help identify the source of the crosstalk by measuring the spur amplitude as a function of f_0. Equation (5) also reveals the tolerable crosstalk for a required SFDR. For example, to achieve an interleaving SFDR of 80 dBc, the channel-to-channel crosstalk of the optical demultiplexer must be <-40 dB and the detected voltage must reset to within 10^{-4} of the previous sample value. It is important to note that this crosstalk analysis pertains to both optical time- and wavelength-division demultiplexers, as well as electronic demultiplexers.

The phase-encoded optical sampling technique has also enabled a new tool for characterizing the timing jitter of short-pulse optical sources [11]. Since the technique provides extraordinary suppression (60 dB) of laser amplitude noise, it allows the laser phase noise or timing jitter to be independently observed and quantified. The measurement involves sampling a high-frequency signal to efficiently convert the laser's timing jitter into amplitude noise in the estimate of the sampled signal voltage. A timing-jitter variance is then determined from the signal frequency and the SNR of the sampled signal. The technique allows both pulse-to-pulse jitter and periodic-pattern (supermode) jitter in harmonically mode-locked lasers to be observed. Measurements performed by sampling a 3-GHz sinusoid with the harmonically mode-locked erbium-doped fiber laser described above revealed that the laser's wide-band pulse-to-pulse jitter and the rms periodic-pattern jitter are less than 50 and 70 fs, respectively. The pulse-to-pulse jitter value is an upper bound since it includes the phase noise of the synthesizer used to generate the 3-GHz input sinusoid. The sample-to-sample jitter of the 3-GHz sinusoid was estimated to be $\sim$50 fs, implying that the actual wide-band laser jitter is much smaller than the above calculated value. This jitter measurement technique is especially useful for characterizing optical pulse sources used in photonic ADCs since it provides an *in situ* measure of the impact of the laser noise on ADC performance.

IV. 505-MS/s Optically Sampled ADC

A. System Description

Our most recent work involves extending the bandwidth of the phase-encoded sampling technique to $\sim$250 MHz. The 505-MS/s optical sampling system (Fig. 4) consists of a mode-locked fiber laser operating at 505 MHz, a dual-output $LiNbO_3$ MZ modulator ($V_\pi = 3$ V, 3-dB bandwidth $= 3$ GHz), a pair of high-extinction $LiNbO_3$ 1-to-8 optical time-division demultiplexers, and an array of photonic integrate-and-reset (PHIR) circuits followed by 14-b electronic quantizers (Analog Devices AD6644) operating at 63.1 MS/s. The digital samples from each quantizer are stored in 1-Msample buffers and then processed offline. System timing signals are derived from the detected laser output and are distributed to the demultiplexers, PHIR circuits, and quantizers.

As described above, phase-encoded optical sampling of the electrical signal is achieved by transmitting the precisely timed laser-pulse train through the dual-output MZ modulator. The energy of each input pulse is split between the two output ports, as determined by the voltage applied during the time that the pulse traverses the modulator. The 1-to-8 optical demultiplexers are used to rate reduce and distribute the post-sampling pulses to the parallel array of PHIR circuits and electronic quantizers. After digitization, the complementary modulator output samples are combined to invert the interferometer's transfer function and obtain the phase difference in the interferometer arms at the time of pulse transmission. The estimate of the sampled input-voltage is obtained by multiplying the phase difference by the factor V_π/π. Details of the phase-decoding process are provided in the Appendix. The phase-decoded samples are then time interleaved to recover the signal at the front-end sampling rate (505 MS/s).

The optical pulse source is a 1.55-μm polarization-maintaining (PM) erbium-doped fiber ring laser that is harmonically mode locked using 180-ps electrical pulses generated by a GaAs/AlAs resonant tunneling diode (RTD) transmission-line oscillator [48]. Use of the short RTD oscillator pulses allows the laser to generate 30-ps pulses at a relatively low 505-MHz repetition rate (fifty-first cavity harmonic). The RTD oscillator is injection locked at its eleventh harmonic (5.55 GHz) using an HP8665B synthesizer. The laser output is amplified using a PM erbium-doped fiber amplifier (EDFA) having a maximum saturated output power of 200 mW. The PM amplifier uses non-PM erbium-doped fiber in a double-pass configuration [49]. Although no active cavity stabilization was used for these measurements, excellent side-mode suppression ($>$65 dB) was observed.

The Ti-indiffused $LiNbO_3$ 1-to-8 optical demultiplexers employ a high-extinction design (Fig. 5) to minimize crosstalk between parallel channels. Each of the seven demultiplexer-switch

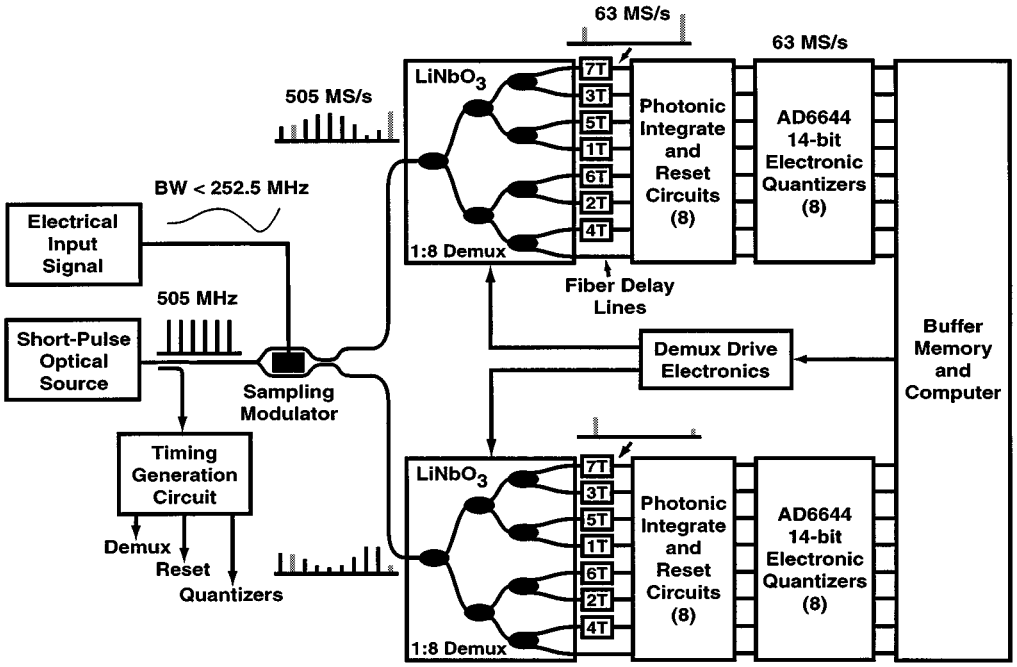

Fig. 4. Block diagram of the 505-MS/s optically sampled ADC consisting of a mode-locked laser pulse source, a dual-output sampling modulator, a pair of high-extinction 1-to-8 $LiNbO_3$ optical time-division demultiplexers, and an array of PHIR circuits followed by 14-b electronic quantizers.

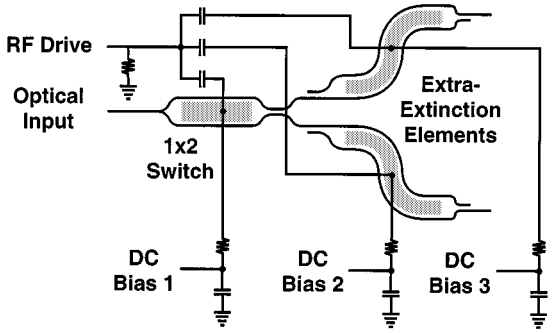

Fig. 5. Three-element stage used in the 1-to-8 $LiNbO_3$ optical demultiplexer and consisting of a 1×2 switch followed by a pair of extra-extinction modulators. The three elements have a common RF drive and individual dc biases. Waveguide bend radii are exaggerated for illustration.

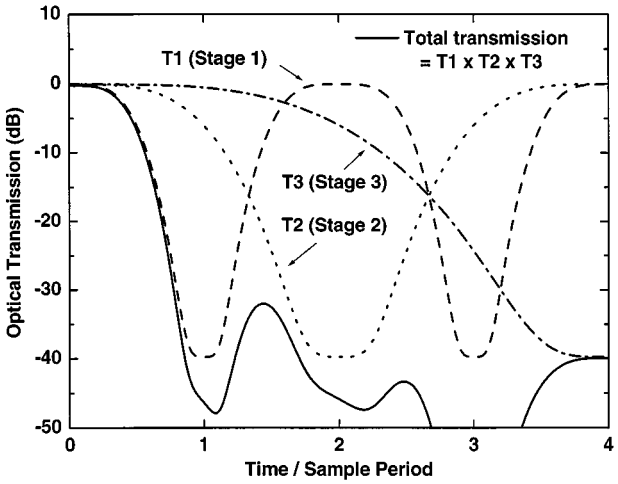

Fig. 6. Theoretical optical transmission versus time of one channel of the 1-to-8 optical demultiplexer driven by phased sinusoids. Analysis assumes a 20-dB extinction per element and a 5% mismatch in V_π between the switch and extinction elements in each stage.

stages consists of a 1×2 switch element with an extra extinction modulator at each output arm. The stages are driven using phased sinusoids with the three elements of a given stage driven by a common signal. The extinction for a single stage ranges between 36–46 dB. The 3-dB bandwidth of a stage is 600 MHz. The half-wave voltages (V_πs) vary from 6.5 to 7.4 V with $<2.5\%$ variation within a single stage. The total channel insertion loss ranges from 6.8 to 8.4 dB.

Fig. 6 shows the theoretical optical transmission versus time for a 1-to-8 demultiplexer channel having 20-dB extinction per element and a 5% mismatch in V_π between the switch and extinction element. The pulse of interest is transmitted at sample time $T = 0$ and the pulses that must be rejected to minimize channel-to-channel crosstalk are transmitted at $T = 1, 2, \ldots, 7$. Only half of the eight-sample sequence is shown since the transmission is symmetric around $T = 4$. The transmission curves reveal that the crosstalk of the sinusoidal drive scheme is limited to the approximately -40-dB crosstalk of stage 3 at $T = 4$. The curves also show that the scheme is fairly insensitive to timing errors and V_π mismatch within a stage. For the 505-MS/s system, the relative timing between the sampling pulses and drive signals can be off by ± 250 ps before the crosstalk of the $T = 1$ pulse is greater than -40 dB. The 5% V_π mismatch included in the calculation has little effect on the demultiplexer's transmission characteristic, indicating that the measured mismatch of 2.5% should not degrade system performance.

The PHIR circuits (Fig. 7) are used to convert the energy of the optical pulses to voltage levels compatible with the electronic quantizer inputs. The pulses are detected with graded-heterojunction InGaAs/InP p-i-n photodiodes having 50-μm diam-

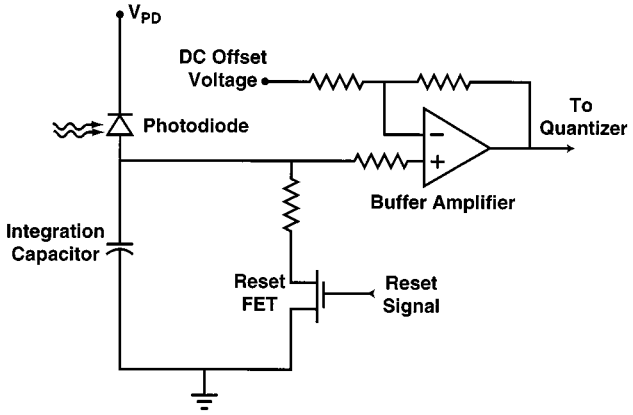

Fig. 7. PHIR circuit consisting of an InGaAs photodiode, an integration capacitor, a buffer amplifier, and a reset FET. The dc offset voltage is used to align the PHIR output with the quantizer voltage range.

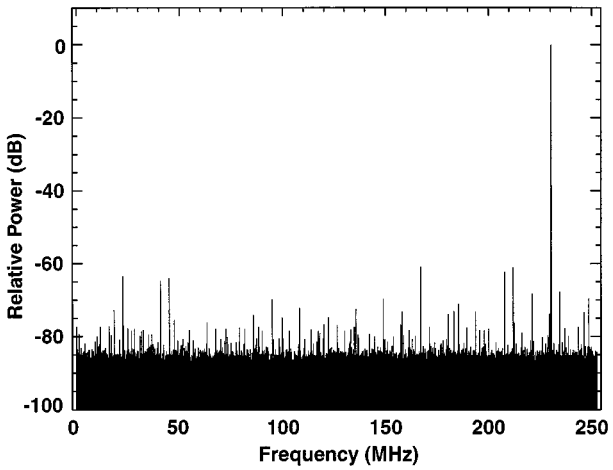

Fig. 8. Spectrum of a sinusoidal signal (f $=$ 224.86 MHz, m $=$ $V_{\mathrm{IN},\,P-P}/V_\pi = 15\%$) measured using the 505-MS/s optically sampled ADC. FFT size $=$ 256K samples.

eter and responsivity of 0.7–0.8 A/W at 1550 nm. During the detection phase, the circuit's reset FET is off and the pulsed photodiode current is integrated in a 12-pF capacitor. The integrated voltage is then buffered and level shifted to match the quantizer's $\pm$1-V input range. After allowing $\sim$10 ns for amplifier settling, the quantizers are simultaneously clocked to digitize the output voltages. The fiber delay lines included at the demultiplexer outputs are used to time align the pulses at the PHIR circuit inputs so that a single reset and a single quantizer clock can be used to control the entire array. It is important to note that the system's sampling accuracy is determined at the sampling modulator and not at the quantizer. Since the integrated voltage is slowly varying when the quantizer is clocked, timing jitter on the quantizer clock does not introduce a large error. After the quantizers have been clocked, the reset FET is switched on for 4 ns ($\sim$10 times the reset-circuit time constant) to drain the integrated photocurrent from the integration capacitor.

The ADC system must be properly initialized and calibrated to optimize both the phase-encoded sampling and converter time-interleaving techniques. Since each of the 42 MZ interferometers on the pair of demultiplexers has two free parameters (dc bias and V_π) and each of the 16 time-interleaved channels has two parameters (offset and gain), a total of 116 parameters need to be measured and set. Some of the parameters, such as V_π, are fixed by the hardware design and are time invariant. The demultiplexers are configured by: 1) sweeping the dc biases and fitting the measured responses to determine the dc-bias points and 2) varying the RF drive voltages to maximize the transmission of the desired pulse. The channel offsets are determined by measuring the PHIR output voltages with the laser off. The relative channel gains are measured by sampling a calibration tone, Fourier transforming the sampled data, and calculating the relative amplitudes of the appropriate frequency bin.

System setup and data collection are performed using electronic boards housed in a VMEbus chassis. The 16 AD6644 electronic quantizers required for the 1-to-8 phase-encoded system are integrated onto four boards each having four quantizers per board. Two digital-to-analog converter (DAC) boards are used to control: 1) the dc biases for the 42-switch and extinction elements on the pair of 1-to-8 demultiplexers and 2) the attenuators that set the ac drive amplitude for the 14 three-element stages on the demultiplexers. An interface board connects the VMEbus chassis to a Pentium-class computer that controls the overall system and processes the collected samples.

B. Initial Measurement Results

Fig. 8 shows the Nyquist-bandwidth power spectrum of a sinusoidal test signal sampled with the 505-MS/s optical sampling system. The signal power at the sampling modulator's 28-Ω input termination was -2.9 dBm, corresponding to modulation index of $m = 15\%$. The signal frequency (224.86 MHz) was selected to be in the center of a fast Fourier transform (FFT) bin to avoid the need for windowing. The average laser power at the input to the modulator was 100 mW. The spectrum in Fig. 8 reveals that the overall system SFDR is presently limited to 61 dB by interleaving spurs that result from channel-to-channel mismatch and crosstalk errors (see the above crosstalk discussion). The SNR of the sampled signal in Fig. 8 is 41 dB. The dependence of the SNR on the laser power and the modulation index is discussed below. For the current 505-MS/s ADC, supermode noise produced by the harmonically mode-locked fiber laser does not degrade either the SFDR or SNR. Most of the supermode noise energy ($>$95%) is amplitude noise that is eliminated by the phase-encoded sampling technique. The remaining phase-noise component can introduce periodic pattern spurs when high-frequency signals are sampled. However, signal frequencies as high as 3 GHz have been sampled using the current laser without degrading the SFDR or the SNR [11].

The high linearity of the phase-encoded sampling process is illustrated by the 78-dB two-tone IM3 of the data in Fig. 9 (note the reduced frequency range). For this measurement, the tone frequencies were 224.86 and 230.04 MHz, and the input power of each tone was -2.9 dBm (single-tone $m = 15\%$). This value of IM3 represents an improvement of 29 dB relative to the theoretical IM3 for a single-output amplitude modulator sampling a signal with a 15% modulation index. The IM3 of the current system is constrained by saturation of the 50-μm photodiodes. The peak optical intensity at the photodiodes was greater than 10 kW/cm^2. Since the integration time of the PHIR circuit

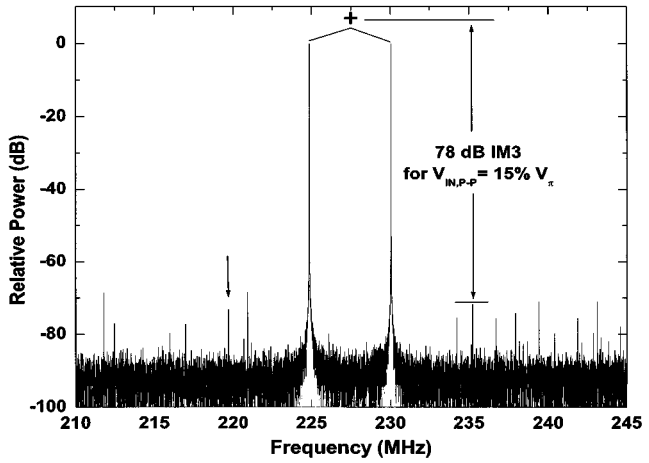

Fig. 9. Portion of a two-tone spectrum measured using the 505-MS/s optically sampled ADC, showing a 78-dB IM3 suppression ratio. IM3 spurs indicated by arrows. Signal frequencies = 224.86 and 230.04 MHz. Input power of each tone = −2.9 dBm ($m \sim 0.15$). Optical power at modulator input = 100 mW. FFT size = 256K samples.

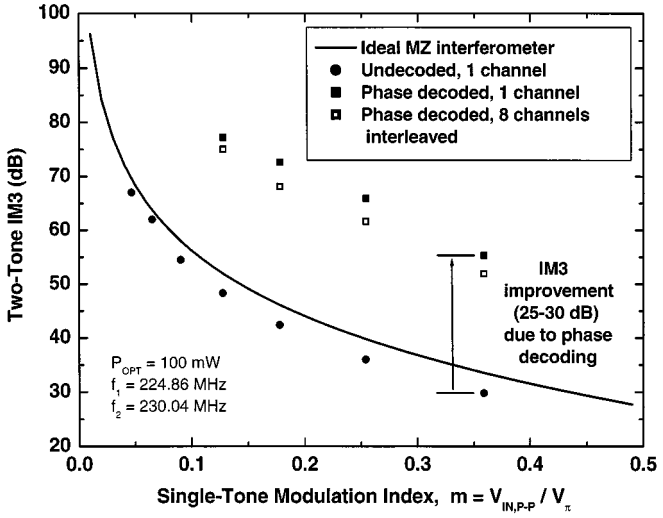

Fig. 10. Measured two-tone IM3 versus single-tone modulation index of the 505-MS/s optically sampled ADC for undecoded single-channel, phase-decoded single-channel, and eight phase-decoded interleaved channels. IM3 associated with the nonlinearity of an ideal MZ interferometer is also shown (solid line). The optical power at the modulator input is 100 mW.

(10 ns) is significantly larger than the optical pulsewidth (30 ps), the nonlinearity arises due to saturation of the photodiode responsivity (i.e., average number of carriers generated per incident photon) and not pulse distortion effects [50]. As mentioned above, an IM3 of 87 dB was obtained for a 208-MS/s ADC operating under similar conditions when photodiodes having a 300-μm diameter were used [47].

The data of Fig. 10 reveal that the improvement of the two-tone IM3 due to phase-encoded optical sampling is 25–30 dB for single-tone modulation indexes in the range of $m = 0.1$ to 0.35. Note that m must be <0.5 to keep the two-tone modulation index <1.0 so that the inversion of the MZ transfer function is unique. In practice, m is limited by residual calibration errors and system noise that prohibit phase decoding by causing the argument of the $\sin^{-1}(\,)$ function in (4) to exceed ± 1. Fig. 10 also shows that the IM3 of the undecoded (i.e., intensity sampled) data is slightly worse than the IM3 associated with the nonlinearity of an ideal MZ interferometer (solid line). This observation indicates that there is another source of nonlinearity in the system, which we currently attribute to the photodetectors. The IM3 of a time-interleaved system will be dominated by the channel with the worst IM3. In the 1-to-8 system, the IM3 of the best channel was 2–5 dB better than that of the full interleaved system (Fig. 10).

The SNR of the phase-encoded sampling technique is determined by the modulation depth, the average laser power, and the noise associated with the laser, signal source, detection electronics, and quantizers. Laser amplitude noise is negligible due to the amplitude noise suppression inherent in the phase-decoding process. Since our system uses a mode-locked fiber laser with timing jitter <50 fs, noise due to timing jitter can be ignored to the 12-b level for input signal frequencies below 1 GHz (refer to Fig. 1).

An analysis was performed to determine the SNR of the 1-to-8 ADC as a function of laser pulse energy E_0 at the modulator input and modulation index m (see the Appendix for details). The analysis includes the effects of shot noise and detection/quantization noise. It does not include distortion due to interleaving spurs and nonlinearities. The quantization noise was determined by measuring the average noise generated by the 16 quantizers with their inputs terminated. The measured 10.5 effective bits is 1.5 bits (9 dB) lower than that specified for the AD6644 quantizers, indicating an SNR degradation due to the present input signal conditioning on the quantizer boards. The light-independent noise due to the PHIR detection electronics was determined to be negligible by repeating the quantizer noise measurement with the quantizer inputs connected to the PHIR circuit outputs and the laser input disconnected. Other system parameters included in the analysis are the average optical transmission (-12 dB) due to the excess loss in the sampling modulator and 1-to-8 demultiplexers, the photodiode external quantum efficiency (0.55), and a total integration capacitance (23 pF) that includes both the intended capacitance (12 pF) and an estimate of the parasitic capacitance (11 pF). The analysis also assumes that the amplitude of the PHIR output signal is constrained to be within the full-scale input range of the quantizer under both light and no-light conditions.

The analysis results in Fig. 11 reveal that the SNR can be increased by increasing either the optical pulse energy or the modulation index, but only over a limited range. For a given modulation depth, the SNR increase is proportional to the square of the pulse energy up to the point where the detected voltage exceeds the ADC maximum input voltage. The SNR where this "clipping" occurs is dependent on the modulation index. For our current 1-to-8 system parameters, the theoretical SNR is always quantization-noise limited. Therefore, increasing the modulation index improves the SNR only up to $m \sim 0.6$ due to the nonlinear noise enhancement inherent in the phase-decoding process. At higher modulation depths, the theoretical SNR actually decreases (see the $m = 0.8$ case in Fig. 11). Details of this nonlinear noise-enhancement effect are provided in the Appendix.

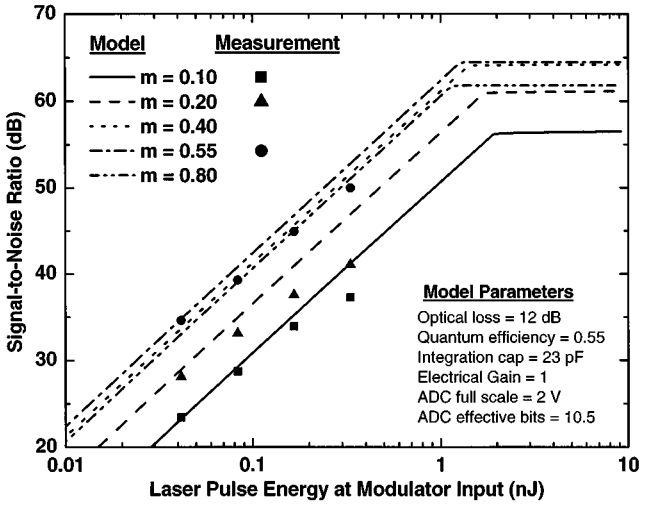

Fig. 11. Theoretical and measured SNR of the 505-MS/s optically sampled ADC versus laser pulse energy and modulation index (m). Deviation between measured data and model at high optical pulse energy is due to *increased noise* and not signal saturation.

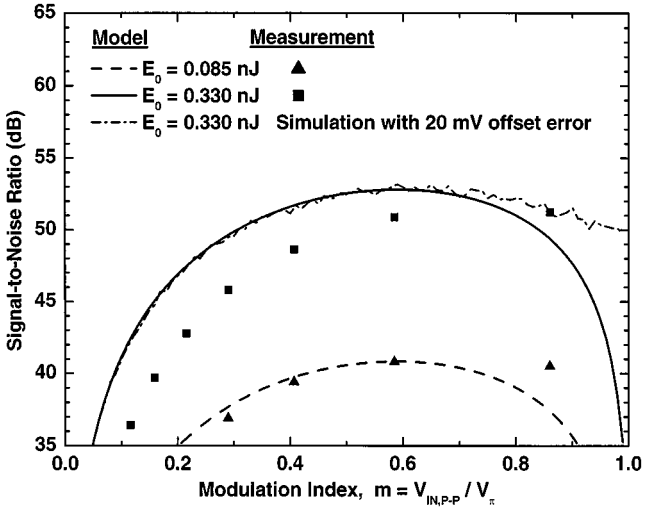

Fig. 12. Theoretical and measured SNR of the 505-MS/s optically sampled ADC versus modulation index (m) for two different pulse energies ($E_0 = 0.085$ and 0.33 nJ). Simulated result shows that an offset voltage error mitigates the predicted SNR reduction at high modulation indexes.

Fig. 11 also shows the results of the measured SNR performance of the 505-MS/s system at modulation indexes of $m = 0.10$, 0.20, and 0.55. To be consistent with the calculated SNR values, the measured SNR values do not include interleaving spurs and nonlinear distortion. At the smallest pulse energy ($E_0 = 0.04$ nJ), the measured and calculated SNR values are nearly identical. However, as the pulse energy increases, the difference between the measured and calculated SNR values increases with a maximum difference of 6 dB at $E_0 = 0.33$ nJ. Thus, the measured data show a limiting effect not included in the SNR analysis. The measured SNR degradation results from *increased noise* and not decreased signal since the undecoded signal powers do not show any evidence of saturation. The likely source of the additional nose is amplified spontaneous emission (ASE) noise from the PM EDFA. ASE noise is not included in the present SNR analysis. For the measured date in Fig. 11, the pulse energy was varied by varying the EDFA pump power. Subsequent measurements have shown that as the pump power is increased, both the pulse power and the ASE noise power increase, but the optical SNR actually *decreases*. This decrease in optical SNR with increasing pump power was exaggerated by the absence of an optical filter between the EDFA output and the sampling modulator input. Another possible cause of the increased noise is the large excess intensity noise associated with the double-pass PM EDFA architecture relative to that of the single-pass EDFA design [51].

The SNR analysis presented here predicts that the noise-enhancement effect should cause the SNR to decrease with increasing modulation index for $m > 0.6$. However, the measured data do not show a strong SNR decrease as m approaches one (Fig. 12). At low optical-pulse energy ($E_0 = 0.085$ nJ), only a small SNR decrease (0.3 dB) is observed as m is increased from 0.6 to 0.85, while at higher optical-pulse energy ($E_0 = 0.33$ nJ), the SNR actually increases slightly (0.3 dB) to 51 dB. This 51-dB SNR is the largest that has been obtained with the 505-MS/s system. The corresponding predicted reduction in SNR is about 3 dB for both pulse energies. The difference between the measured and predicted SNR decrease is likely due to the ideal system assumed in the SNR analysis. If nonidealities such as offset voltage errors and sample-to-sample leakage are taken into account, the impact of the noise-enhancement effect is greatly reduced. A full simulation of the phase-encoded sampling system including Gaussian-distributed noise shows that a 20-mV offset voltage error mitigates the SNR reduction at high modulation depths (see Fig. 12). Without the offset error, the simulated result (not shown) has the same SNR versus m dependence as that of the SNR analysis.

V. Conclusions

In this paper, we have reemphasized the potential improvements to ADC technology that can be achieved through optical sampling techniques. The principal advantage of optical sampling is the low timing jitter of advanced mode-locked lasers relative to that of electronic sampling clocks. The narrow-band jitter of actively mode-locked fiber lasers (<10 fs) has been shown to be limited by the phase noise of the laser's electronic reference oscillator, and pulse-to-pulse jitter estimates (<50 fs) indicate the absence of a significant wide-band-noise component. Therefore, optical pulse sources with quantum-limited pulse-to-pulse jitter of <10 fs may be realizable through proper design and the use of low-noise reference oscillators. The low back-electromotive force (EMF) of electrooptic sampling transducers facilitates the accuracy of the optical sampling process by providing high isolation between the optical clock pulses and the signal being sampled. Another advantage of optically sampled ADCs is that the sampling operation can be viewed as a near-perfect mixer, allowing microwave signals to be directly down-converted in the ADC component. For a given jitter-limited resolution, the maximum frequency that can be sampled is limited only by the bandwidth of the sampling modulator and the temporal width of the optical pulses. Thus, it is feasible to undersample signals with frequencies in the

range of 100 GHz with 6-b resolution (assuming ∼10-fs jitter) using demonstrated modulator and mode-locked laser technologies. Other advantages of optical sampling include remote sampling enabled by low-loss optical fibers and the availability of low-crosstalk optical demultiplexers to improve time-interleaved ADCs.

The phase-encoded sampling technique that we have developed provides both excellent linearity and nearly complete rejection of laser amplitude noise. An improvement of 25–30 dB in two-tone IM3 relative to intensity sampling has been demonstrated. We expect the linearity of this technique to be enhanced through the use of photodiodes with higher saturation intensities and by minimizing residual calibration errors. The impact of laser intensity noise on the system SNR performance is mitigated by 60 dB of amplitude noise suppression.

The amplitude noise suppression attained via phase-encoded optical sampling also minimizes the impact of supermode noise associated with the use of harmonically mode-locked lasers. Supermode intensity fluctuations are rejected, leaving only contributions due to supermode phase or timing noise. As mentioned earlier, we have shown that this supermode phase noise does not degrade ADC performance when sampling a 3-GHz signal using a 208-MS/s harmonically mode-locked fiber laser. It is expected that similar sampling quality can be obtained at much higher rates. Indeed, a 40-GS/s regeneratively FM mode-locked fiber laser [52] has demonstrated side-mode suppression (70 dB) exceeding that of our 208-MS/s laser.

In our ADC architecture, the potential of real-time phase decoding [i.e., implementation of (4)] is enabled through the use of parallel channels. We believe that current detection electronics and digital signal processing hardware will support real-time operation at a few hundred megasamples per second per parallel channel. Aggregate real-time sampling rates of a few gigasamples per second may then be achieved by using 8 or 16 parallel channels.

The initial performance our 505-MS/s ADC reveals that effort is still required before the full benefits of optical sampling will be realized. The primary challenge is to maintain the high-quality sampling information, present at the output of the sampling modulator, through the optical demultiplexing, detection, and quantization stages. The present SNR of 51 dB (8.2 bits) is quantizer-noise limited, and would immediately increase by 9 dB (1.5 bits) if the performance of the current quantizer boards matched the specified performance of the AD6644 converters used. Increasing the laser power and sampling modulation depth to better utilize the full-scale range of the quantizers will provide further improvements in SNR. The overall SFDR is limited to 61 dB by interleaving spurs attributed to residual crosstalk errors. We believe that the current performance limits can be overcome and that 12-b optically sampled ADCs operating at mutligigahertz rates can be realized.

APPENDIX
SIGNAL-TO-NOISE ANALYSIS

Assuming that: 1) both the optical pulse's width and time of propagation through the modulator are much smaller than the period of the highest frequency being sampled and 2) the modulator on/off extinction ratio is infinite, the pulse energies at the complementary output ports of the MZ sampling modulator due to a single input pulse can be written as

$$E_A = \frac{(E_0 + \Delta E)}{2}\left(1 + \sin\phi_{\mathrm{IN}}\right) \tag{6}$$

$$E_B = \frac{(E_0 + \Delta E)}{2}\left(1 - \sin\phi_{\mathrm{IN}}\right) \tag{7}$$

where E_0 is the energy of the pulse at the input to the modulator, ΔE is a random variation in the pulse energy, $\phi_{\mathrm{IN}} = \pi \cdot V_{\mathrm{IN}}/V_\pi$ is the phase difference between the two arms of the interferometer assumed to be biased at quadrature, V_{IN} is the voltage applied to the modulator at the instant the pulse passes through the modulator, and V_π is the modulator's half-wave voltage.

In the PHIR detection scheme used here, the optical pulses are converted to charge packets using a photodetector, and the charge is then integrated in a capacitor. Assuming equal channel gains and zero dc offsets or, equivalently, perfect calibration, the resulting voltage signals at the outputs of the electronic quantizers can be written as

$$V_A = \frac{(V_0 + \Delta V)}{2}\left(1 + \sin\phi_{\mathrm{IN}}\right) + v_{nA} \tag{8}$$

$$V_B = \frac{(V_0 + \Delta V)}{2}\left(1 - \sin\phi_{\mathrm{IN}}\right) + v_{nB} \tag{9}$$

where

$$V_0 + \Delta V = \left(T_{\mathrm{OPT}}\,\frac{\eta\lambda_c}{h\,c}\,\frac{q_e}{C_I}\,G\right)(E_0 + \Delta E) \tag{10}$$

where T_{OPT} is the maximum optical transmission between the modulator input and photodetector input, η is the external quantum efficiency of the photodetector, λ_c is the center wavelength of the optical pulse, h is Planck's constant (6.626 $\times$ 10 $^{-34}$ J$\cdot$s), c is the speed of light in vacuum (2.9979 $\times$ 10 ^{8} m/s), q_e is the electron charge (1.602 $\times$ 10 $^{-19}$ C), C_I is the integration capacitance, and G is any additional voltage gain. The terms v_{nA} and v_{nB} are noise voltages associated with shot noise in the photodetector and the total added noise of the detection electronics and quantizers.

The estimate of the interferometer phase angle is decoded from the quantized voltages as

$$\begin{aligned}\phi_{\mathrm{OUT}} &= \sin^{-1}\left(\frac{V_A - V_B}{V_A + V_B}\right)\\ &= \sin^{-1}\left(\frac{(V_0 + \Delta V)\sin\phi_{\mathrm{IN}} + v_{nA} - v_{nB}}{(V_0 + \Delta V) + v_{nA} + v_{nB}}\right).\end{aligned} \tag{11}$$

Note that, for large SNR (i.e., $V_0 \gg v_{nA}$, v_{nB}), the estimate of the phase angle is approximately equal to the input phase angle ($\phi_{\mathrm{OUT}} \approx \phi_{\mathrm{IN}}$) *independent* of any optical pulse energy noise variations ΔE. As described above, amplitude noise suppression of 60 dB has been obtained using this phase-encoded sampling technique [11]. The estimate of the voltage applied to the sampling modulator at the instant of optical pulse arrival is

$$V_{\mathrm{OUT}} = \frac{V_\pi}{\pi}\,\phi_{\mathrm{OUT}}. \tag{12}$$

The variance of $\phi_{\rm OUT}$ is a function of the noise voltage variances $\sigma^2_{v_{nA}}$ and $\sigma^2_{v_{nB}}$. Assuming that v_{nA} and v_{nB} are independent with zero mean, $\sigma^2_{\phi_{\rm OUT}}$ can be expressed as [53]

$$\sigma^2_{\phi_{\rm OUT}} = \left(\frac{\partial \phi_{\rm OUT}}{\partial v_{nA}}\bigg|_{v_{nA}=v_{nB}=0} \right)^2 \sigma^2_{v_{nA}} + \left(\frac{\partial \phi_{\rm OUT}}{\partial v_{nB}}\bigg|_{v_{nA}=v_{nB}=0} \right)^2 \sigma^2_{v_{nB}} = \frac{1}{V_0^2}\left(\frac{1-\sin\phi_{\rm IN}}{1+\sin\phi_{\rm IN}} \cdot \sigma^2_{v_{nA}} + \frac{1+\sin\phi_{\rm IN}}{1-\sin\phi_{\rm IN}} \cdot \sigma^2_{v_{nB}} \right) \tag{13}$$

and the variance of the estimated input voltage is

$$\sigma^2_{V_{\rm OUT}} = \left(\frac{V_\pi}{\pi}\right)^2 \sigma^2_{\phi_{\rm OUT}}. \tag{14}$$

Note that the expression for $\sigma^2_{\phi_{\rm OUT}}$ does not depend on the variance of the pulse energy fluctuations $\sigma^2_{\Delta E}$ for the case of perfect calibration. The dependence of $\sigma^2_{\phi_{\rm OUT}}$ on the input phase angle $\phi_{\rm IN}$ and, hence, on the applied voltage $V_{\rm IN}$, is different for the cases of shot noise and uncorrelated detection/quantization noise:

1) Photodetector Shot Noise: Assuming that the shot noise is Poisson distributed, the variance in the number of detected electrons σ^2_N is equal to the mean number of detected electrons N [53]. For the pulses from the complementary modulator outputs, the detected electron variances are

$$\sigma^2_{N_A} = N_A = \frac{N_0}{2}(1+\sin\phi_{\rm IN}) \tag{15}$$

$$\sigma^2_{N_B} = N_B = \frac{N_0}{2}(1-\sin\phi_{\rm IN}) \tag{16}$$

where

$$N_0 = \left(T_{\rm OPT}\frac{\eta\lambda_c}{hc}\right)E_0. \tag{17}$$

The shot-noise voltage variances can then be written as

$$\sigma^2_{v_{nA}} = \left(\frac{q_e}{C_I}G\right)^2 \frac{N_0}{2}(1+\sin\phi_{\rm IN}) \tag{18}$$

$$\sigma^2_{v_{nB}} = \left(\frac{q_e}{C_I}G\right)^2 \frac{N_0}{2}(1-\sin\phi_{\rm IN}). \tag{19}$$

Substituting (18) and (19) into (13) gives

$$\sigma^2_{\phi_{\rm OUT}} = \frac{1}{N_0} \text{ for detector shot noise.} \tag{20}$$

Equation (20) reveals that $\sigma^2_{\phi_{\rm OUT}}$ is independent of $\phi_{\rm IN}$ for the case of shot noise. The reason for this independence is that the total average energy output from the modulator is a constant, i.e., $E_A + E_B = E_0$. Therefore, as $\phi_{\rm IN}$ changes, the variance of the shot noise in one channel increases while that of the complementary channel decreases.

2) Uncorrelated Detection and Quantizer Noise: Assuming that the noise added by the each of the two detection circuits and quantizers is uncorrelated and equal with a variance of

$$\sigma^2_{v_Q} = \sigma^2_{v_{nA}} = \sigma^2_{v_{nB}} \tag{21}$$

then (13) becomes

$$\sigma^2_{\phi_{\rm OUT}} = \frac{1}{V_0^2}\left(\frac{1-\sin\phi_{\rm IN}}{1+\sin\phi_{\rm IN}} + \frac{1+\sin\phi_{\rm IN}}{1-\sin\phi_{\rm IN}}\right)\sigma^2_{v_Q}, \quad \text{for uncorrelated quantizer noise.} \tag{22}$$

Equation (22) shows that $\sigma^2_{\phi_{\rm OUT}}$ is a function of $\phi_{\rm IN}$ and, hence, the applied voltage $V_{\rm IN}$. When $\phi_{\rm IN}$ is small, $\sigma^2_{\phi_{\rm OUT}} = (2/V_0^2)\sigma^2_{v_Q}$, but as $\sin\phi_{\rm IN}$ approaches either $+1$ or -1, the variance of the decoded $\phi_{\rm OUT}$ approaches infinity. This increase in $\sigma^2_{\phi_{\rm OUT}}$ is a direct consequence of the nonlinearity of the $\sin^{-1}(\,)$ function inherent in the phase-decoding process in (11).

Up to this point, we have examined $\sigma^2_{\phi_{\rm OUT}}$ as a function of a fixed value of $\phi_{\rm IN}$. Now consider the case of a time-varying sinusoidal input signal

$$\phi_{\rm IN}(t) = \frac{\pi}{V_\pi}V_{\rm IN}(t) = \frac{\pi}{V_\pi}\frac{V_{\rm IN,\,P-P}}{2}\sin(2\pi t/T_0) \tag{23}$$

where $V_{IN,\,\rm P-P}$ is the peak-to-peak voltage of the input signal and T_0 is the period of the sinusoid. We define the noise enhancement factor (NEF) as a function of the modulation index $m = V_{IN,\,\rm P-P}/V_\pi$ by integrating the $\phi_{\rm IN}$-dependent part of (22) over one cycle of the sinusoid

$$\text{NEF}(m) = \frac{1}{2T_0}\int_0^{T_0}\left(\frac{1-\sin\phi_{\rm IN}(t)}{1+\sin\phi_{\rm IN}(t)} + \frac{1+\sin\phi_{\rm IN}(t)}{1-\sin\phi_{\rm IN}(t)}\right)dt. \tag{24}$$

The NEF represents the increase of the decoded noise variance relative to the small modulation limit. Fig. 13 shows the NEF computed from (24) as a function of m. This noise enhancement limits the useful modulation index in a phase-encoded optical sampling ADC, as discussed in Section IV. At a modulation index of $m = 0.5$, the NEF is approximately two. For $m > 0.5$, the NEF increases rapidly, overwhelming any SNR improvement due to the increased signal power associated with larger m.

Once the phase-decoded output signal and the shot-noise and detection/quantization-noise variances have been determined, the SNR is calculated using

$$\text{SNR} = \frac{(V_{\rm OUT,\,RMS})^2}{(\sigma^2_{V_{\rm OUT}})_{\rm SHOT} + (\sigma^2_{V_{\rm OUT}})_{\rm DET/QUANT}} \tag{25}$$

where $V_{\rm OUT,\,RMS}$ is the rms value of the decoded output voltage.

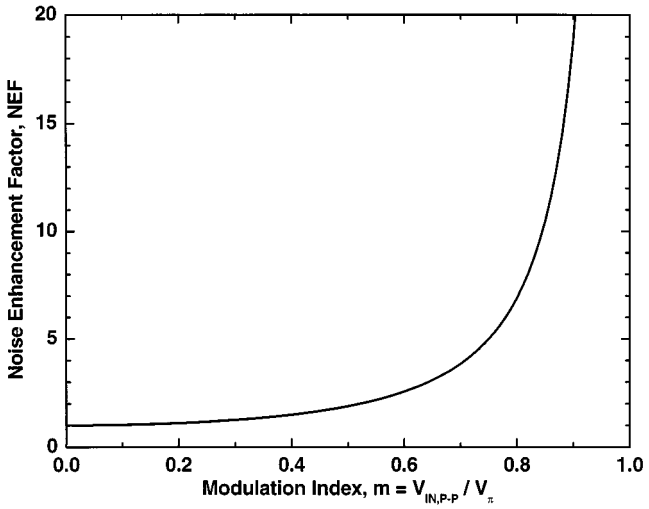

Fig. 13. NEF associated with the phase-encoded sampling technique as a function of modulation index. Analysis assumes that the electrical input signal is sinusoidal.

The SNR analysis can be greatly simplified when the modulation depth is small and the electronic quantizer is the dominant noise source. Under these conditions, the SNR of the phase-encoded optical sampling technique can be expressed in decibels as

$$\mathrm{SNR} = \mathrm{SNR}_Q - 20\log_{10}\left(\frac{V_{\mathrm{DET,\,P-P}}}{V_{\mathrm{FS}}}\right) + 3.0\ \mathrm{dB} \qquad (26)$$

where SNR_Q is the full-scale SNR of the two quantizers (assumed to be identical here), $V_{\mathrm{DET,\,P-P}} = V_{A,\,\mathrm{P-P}} = V_{B,\,\mathrm{P-P}}$ is the peak-to-peak detected voltage at the input to the quantizers, and V_{FS} is the full-scale voltage range of the quantizers. Note that $V_{\mathrm{DET,\,P-P}}$ must be less than or equal to V_{FS}. This intuitive equation shows that the SNR of the phase-encoded sampling technique is maximized by generating a detected signal that fills the electronic quantizer's full-scale range through the proper combination of optical power, modulation depth, photodiode efficiency, integration capacitance, and electrical gain. Also note that the SNR of the phase-decoded output signal is always 3 dB larger than the SNR of a single quantizer for a given value of $V_{\mathrm{DET,\,P-P}}$. This half-bit of improvement results because the outputs of two quantizers are combined to obtain the phase-decoded output: the detected signals at the quantizer inputs add coherently, while the uncorrelated quantizer noises add in quadrature.

ACKNOWLEDGMENT

The authors would like to acknowledge the expert assistance of C. Parker, Lincoln Laboratory, Massachusetts Institute of Technology (MIT), Lexington, K. Percival, Lincoln Laboratory, MIT, Lexington, C. Jones, Lincoln Laboratory, MIT, Cambridge, M. Seaver, Lincoln Laboratory, MIT, Lexington, and B. Reynolds, Lincoln Laboratory, MIT, Lexington, in the development of the PHIR detection circuitry and the timing generation components and circuitry. The authors are also grateful for technical discussions with E. Daniel, Mayo Foundation, Rochester, MN, and K. Buchs, Mayo Foundation, Rochester, MN, and the research groups of Prof. E. Ippen, MIT, Cambridge, Prof. H. Haus, MIT, Cambridge, and Prof. R. Ram, MIT, Cambridge.

REFERENCES

[1] R. H. Walden, "Analog-to-digital converter survey and analysis," *IEEE J. Select. Areas Commun.*, vol. 17, pp. 539–549, Apr. 1999.
[2] Analog Devices, Norwood, MA, Analog Devices AD6644 specification sheet, 1999.
[3] W. C. Black and D. A. Hodges, "Time-interleaved converter arrays," *IEEE J. Solid-State Circuits*, vol. SC-15, pp. 1022–1029, Dec. 1980.
[4] C. Schiller and P. Byrne, "A 4-GHz 8-b ADC system," *IEEE J. Solid-State Circuits*, vol. 26, pp. 1781–1789, Dec. 1991.
[5] C. S. G. Conroy, "An 8-b 85-MS/s parallel pipeline A/D converter in 1-μm CMOS," *IEEE J. Solid-State Circuits*, vol. 28, pp. 447–454, Apr. 1993.
[6] K. Poulton, K. L. Knudsen, J. Kerley, J. Kang, J. Tani, E. Cornish, and M. VanGrouw, "An 8-GS/s 8-bit ADC system," in *Proc. VLSI Circuits Symp. Dig.*, 1997, pp. 23–24.
[7] Y.-C. Jenq, "Digital spectra of nonuniformly sampled signals: A robust sampling time offset estimation algorithm for ultra-high-speed waveform digitizers using interleaving," *IEEE Trans. Instrum. Meas.*, vol. 39, pp. 71–75, Feb. 1990.
[8] A. Petraglia and S. K. Mitra, "Analysis of mismatch effects among A/D converters in a time-interleaved waveform digitizer," *IEEE Trans. Instrum. Meas.*, vol. 40, pp. 831–835, Oct. 1991.
[9] R. C. Williamson, P. W. Juodawlkis, J. L. Wasserman, G. E. Betts, and J. C. Twichell, "Effects of crosstalk in demultiplexers for photonic analog-to-digital converters," *J. Lightwave Technol.*, vol. 19, pp. 230–236, Feb. 2001.
[10] T. R. Clark, T. F. Carruthers, P. J. Matthews, and I. N. Duling, III, "Phase-noise measurements of ultrastable 10 GHz harmonically mode-locked fiber laser," *Electron. Lett.*, vol. 35, pp. 720–721, 1999.
[11] P. W. Juodawlkis, J. C. Twichell, J. L. Wasserman, G. E. Betts, and R. C. Williamson, "Measurement of mode-locked laser timing jitter by use of phase-encoded optical sampling," *Opt. Lett.*, vol. 26, pp. 289–291, 2001.
[12] A. E. Siegman and D. J. Kuizenga, "Proposed method for measuring picosecond pulse widths and pulse shapes in CW mode-locked lasers," *IEEE J. Quantum. Electron.*, vol. QE-6, pp. 212–215, Apr. 1970.
[13] D. H. Auston, "Picosecond optoelectronic switching and gating in silicon," *Appl. Phys. Lett.*, vol. 26, pp. 101–103, 1975.
[14] H. F. Taylor, "An electrooptic analog-to-digital converter," *Proc. IEEE*, vol. 63, pp. 1524–1525, Oct. 1975.
[15] ——, "An optical analog-to-digital converter—Design and analysis," *IEEE J. Quantum. Electron.*, vol. QE-15, pp. 210–216, Apr. 1979.
[16] R. A. Becker, C. E. Woodward, F. J. Leonberger, and R. C. Williamson, "Wide-band electrooptic guided-wave analog-to-digital converters," *Proc. IEEE*, vol. 72, pp. 802–818, July 1984.
[17] J. A. Bell, M. C. Hamilton, and D. A. Leep, "Optical sampling and demultiplexing applied to A/D conversion," *Devices for Optical Processing*, vol. 1562, pp. 276–280, 1991.
[18] J. A. Bell, M. C. Hamilton, D. A. Leep, H. F. Taylor, and Y.-H. Lee, "A/D conversion of microwave signals using a hybrid optical/electronic technique," *Opt. Technol. Microwave Applicat. V*, vol. 1476, pp. 326–329, 1991.
[19] M. Y. Frankel, J. U. Kang, and R. D. Esman, "High-performance photonic analogue–digital converter," *Electron. Lett.*, vol. 33, pp. 2096–2097, 1997.
[20] J. U. Kang, M. Y. Frankel, and R. D. Esman, "Highly parallel pulsed optoelectronic analog–digital converter," *IEEE Photon. Technol. Lett.*, vol. 10, pp. 1626–1628, Nov. 1998.
[21] J. U. Kang and R. D. Esman, "Demonstration of time-interweaved photonic four-channel WDM sampler for hybrid analogue–digital converter," *Electron. Lett.*, vol. 35, pp. 60–61, 1999.
[22] A. S. Bhushan, F. Coppinger, S. Yegnanarayanan, and B. Jalali, "Non-dispersive wavelength-division sampling," *Opt. Lett.*, vol. 24, pp. 738–740, 1999.
[23] T. R. Clark, J. U. Kang, and R. D. Esman, "Performance of a time- and wavelength-interleaved photonic sampler for analog–digital conversion," *IEEE Photon. Technol. Lett.*, vol. 11, pp. 1168–1170, Sept. 1999.

[24] F. Coppinger, A. S. Bhushan, and B. Jalali, "12 Gsample/s wavelength division sampling analogue-to-digital converter," *Electron. Lett.*, vol. 36, pp. 316–318, 2000.
[25] ——, "Erratum to '12 Gsample/s wavelength division sampling analogue-to-digital converter'," *Electron. Lett.*, vol. 36, p. 1334, 2000.
[26] A. S. Bhushan, F. Coppinger, and B. Jalali, "Time-stretched analogue-to-digital conversion," *Electron. Lett.*, vol. 34, pp. 839–841, 1998.
[27] F. Coppinger, A. S. Bhushan, and B. Jalali, "Photonic time stretch and its application to analog-to-digital conversion," *IEEE Trans. Microwave Theory Tech.*, vol. 47, pp. 1309–1314, July 1999.
[28] A. S. Bhushan, P. Kelkar, and B. Jalali, "30 Gsample/s time-stretch analog-to-digital converter," *Electron. Lett.*, vol. 36, pp. 1526–1527, 2000.
[29] E. Donkor, M. J. Hayduk, R. J. Bussjager, and P. D. Kumavor, "A 2.5 Gb/s flash all-optical analog-to-digital converter," in *Proc. IEEE LEOS Annu. Meeting*, 2000, pp. 204–205.
[30] R. Urata, R. Takahashi, V. A. Sabnis, D. A. B. Miller, and J. S. Harris, "High-speed sample and hold using low temperature grown GaAs MSM switches for photonic A/D conversion," in *Proc. OSA Lasers Electro-Opt. Conf. Tech. Dig.*, Washington, DC, 2001, pp. 66–67.
[31] T. Conese, F. Ricco, M. N. Armenise, C. M. Verber, and R. P. Kenan, "Design of all-optical logic gates in polydiacetylene PTS-clad waveguides," in *Proc. Nonlinear Opt.*, 1998, pp. 352–354.
[32] L. Brzozowski and E. H. Sargent, "All-optical analog-to-digital converters, hardlimiters, and logic gates," *J. Lightwave Technol.*, vol. 19, pp. 114–119, Jan. 2001.
[33] M. J. Hayduk, R. J. Bussjager, and M. A. Getbehead, "Photonic analog to digital conversion techniques using semiconductor saturable absorbers," *Enabling Technol. Aerospace Applicat. II*, vol. 4042, pp. 54–60, 2000.
[34] H. Sakata, "Photonic analog-to-digital conversion by use of nonlinear Fabry–Perot resonators," *Appl. Opt.*, vol. 40, pp. 240–248, 2001.
[35] L. M. Loh and J. L. LoCicero, "Subnanosecond sampling all-optical analog-to-digital converter using symmetric self-electro-optic effect devices," *Opt. Eng.*, vol. 35, pp. 457–466, 1996.
[36] J. Cai and G. F. Taylor, "Demonstration of an optoelectronic 4-bit analog-to-digital converter using a thyristor smart comparator," *Opt. Commun.*, vol. 184, pp. 79–88, 2000.
[37] M. Currie, T. R. Clark, and P. J. Matthews, "Photonic analog-to-digital conversion by distributed phase modulation," *IEEE Photon. Technol. Lett.*, vol. 12, pp. 1689–1691, Dec. 2001.
[38] M. Johansson, B. Löfving, H. Sverker, L. Thylén, M. Mokhtari, U. Westergren, and C. Pala, "Study of an ultrafast analog-to-digital conversion scheme based on diffractive optics," *Appl. Opt.*, vol. 39, pp. 2881–2887, 2000.
[39] B. L. Shoop and J. W. Goodman, "Optical oversampled analog-to-digital conversion," *Appl. Opt.*, vol. 31, pp. 5654–5660, 1992.
[40] P. E. Pace, S. A. Bewley, and J. P. Powers, "Fiber-lattice accumulator design considerations for optical SD analog-to-digital converters," *Opt. Eng.*, vol. 39, pp. 1517–1526, 2000.
[41] L. M. Johnson and H. V. Roussell, "Reduction of intermodulation distortion in interferometric optical modulators," *Opt. Lett.*, vol. 13, pp. 928–930, 1988.
[42] S. A. Hamilton, D. R. Yankelevich, A. Knoesen, R. T. Weverka, and R. A. Hill, "Comparison of an in-line asymmetric directional coupler modulator with distributed optical loss to other linearized electrooptic modulators," *IEEE Trans. Microwave Theory Tech.*, vol. 47, pp. 1184–1192, July 1999.
[43] M. Nazarathy, J. Berger, A. Ley, I. Levi, and Y. Kagan, "Progress in externally modulated AM CATV transmission systems," *J. Lightwave Technol.*, vol. 11, pp. 82–105, Jan. 1993.
[44] Y. Chiu and B. Jalali, "Broad-band electronic linearizer for externally modulated analog fiber-optic links," *IEEE Photon. Technol. Lett.*, vol. 11, pp. 48–50, Jan. 1999.
[45] T. R. Clark, M. Currie, and P. J. Matthews, "Digitally linearized wide-band photonic link," *J. Lightwave Technol.*, vol. 19, pp. 172–179, Feb. 2001.
[46] J. C. Twichell and R. Helkey, "Phase-encoded optical sampling for analog-to-digital converters," *IEEE Photon. Technol. Lett.*, vol. 12, pp. 1237–1239, Sept. 2000.
[47] J. C. Twichell, J. L. Wasserman, P. W. Juodawlkis, G. E. Betts, and R. C. Williamson, "High-linearity 208-MS/s photonic analog-to-digital converter using 1-to-4 optical time-division demultiplexers," *IEEE Photon. Technol. Lett.*, vol. 13, pp. 714–716, July 2001.
[48] E. R. Brown, C. D. Parker, S. Verghese, M. W. Geis, and J. F. Harvey, "Resonant-tunneling transmission-line relaxation oscillator," *Appl. Phys. Lett.*, vol. 70, pp. 2787–2789, 1997.
[49] I. N. Duling, III and R. D. Esman, "Single-polarization fiber amplifier," *Electron. Lett.*, vol. 28, pp. 1126–1128, 1992.
[50] P.-L. Liu, K. J. Williams, M. Y. Frankel, and R. D. Esman, "Saturation characteristics of fast photodetectors," *IEEE Trans. Microwave Theory Tech.*, vol. 47, pp. 1297–1303, July 1999.
[51] P. D. Biernacki, L. T. Nichols, and P. J. Matthews, "Noise effects in polarization maintaining optical amplifiers," in *Proc. Opt. Fiber Commun.*, 2000, pp. 218–220.
[52] M. Nakazawa and E. Yoshida, "A 40-GHz 850-fs regeneratively FM mode-locked polarization-maintaining erbium fiber ring laser," *IEEE Photon. Technol. Lett.*, vol. 12, pp. 1613–1615, Dec. 2000.
[53] A. Papoulis, *Probability, Random Variables, and Stochastic Processes*, 2nd ed. New York: McGraw-Hill, 1984.

Paul W. Juodawlkis (S'86–M'86) was born in Detroit, MI, in 1964. He received the B.S. degree in electrical engineering (*summa cum laude*) from the Michigan Technological University, Houghton, in 1986, the M.S. degree in electrical engineering with a specialization in solid-state circuit design from Purdue University, West Layfayette, IN, in 1988, and the Ph.D. degree in electrical engineering from the Georgia Institute of Technology, Atlanta, in 1999. His doctoral dissertation concerned opto-electronic properties and device applications of low-temperature-grown semiconductor quantum-well materials.

From 1988 to 1993, he was a Technical Staff member at the Lincoln Laboratory, Massachusetts Institute of Technology (MIT), Lexington, where he was a Hardware Systems Engineer involved with a multisensor airborne testbed program. He then joined the Ultrafast Optical Communications Laboratory (UFOCL), Georgia Institute of Technology. In 1999, he rejoined the Lincoln Laboratory, MIT, as a member of the Electro-Optic Materials and Devices Group, and is currently involved in the development of ADCs utilizing optical sampling techniques. His research interests include laser noise characteristics, ultrashort pulse generation and applications, optical nonlinearities, and opto-electronic interfaces.

Dr. Juodawlkis is a member of the IEEE Lasers and Electro-Optics Society (IEEE LEOS), the Optical Society of America, and the American Association for the Advancement of Science (AAAS). He was a recipient of the Georgia Tech President's Fellowship, the Schlumberger Foundation Fellowship, and the International Society for Optical Engineers (SPIE) Scholarship in Optical Engineering.

Jonathan C. Twichell (M'00) received the A.B. degree from Earlham College, Richmond, IN, in 1974, and the M.S. and the Ph.D. degrees in nuclear engineering from the University of Wisconsin-Madison, in 1978 and 1984, respectively. His doctoral dissertation concerned the effects of impurity generation and hydrogen recycling on energy confinement in high-energy-density magnetically-confined plasmas.

After teaching for three years at the University of Oklahoma, he joined the Lincoln Laboratory, Massachusetts Institute of Technology (MIT), Lexington. From 1986 to 1991, he was with the High-Energy Laser Propagation and Control Group, where he designed and implemented wavefront sensors and developed wavefront reconstruction algorithms. From 1991 to 1998, he was a member of the Submicrometer Technology Group, where he was involved with diamond material physics, primarily field- and photo–electron emitters. He is currently the leader of the Electro-Optic Materials and Devices Group, Lincoln Laboratory, MIT. His current research interests center on photonic enhancements to traditional electronic systems and the application of nonlinear systems to wide-band signal processing.

Dr. Twichell is a member of the IEEE Lasers and Electro-Optics Society (IEEE LEOS) and the American Physical Society.

Gary E. Betts (S'84–M'84) received the B.S. degree in physics from Haverford College, Haverford, PA, in 1976, and the M.S. degree in physics and the Ph.D. degree in applied physics from the University of California at San Diego, La Jolla, in 1980 and 1985, respectively. His doctoral dissertation concerned with electrooptic modulators in lithium niobate.

From 1976 to 1978, he was with the Westinghouse Electric Corporation, Baltimore, MD, where he was involved with integrated optics, primarily on the design of geodesic lenses. Since 1985, he has been a Staff Member at the Lincoln Laboratory, Massachusetts Institute of Technology (MIT), Lexington, where he is primarily involved with lithium–niobate integrated-optical modulators and analog fiber-optic links. His research at MIT has included design and fabrication of a variety of lithium–niobate modulators and switch arrays, investigation of drift phenomena in lithium niobate, and research on semiconductor modulators and high-powered semiconductor optical amplifiers.

Dr. Betts is a member of the IEEE Lasers and Electro-Optics Society (IEEE LEOS) and the Optical Society of America.

Jeffrey J. Hargreaves (A'90–M'98) was born in Honolulu, HI, in 1965. He received the Associate degree in computers and electronics from the New Hampshire Vocational Technical College, Nashua, in 1985, the B.S. degree in electrical engineering from the University of Massachusetts, Lowell, in 1995, and the M.S. degree in electrical engineering from the University of New Hampshire, Durham, in 1999. His M.S. thesis concerned intermodulation products due to the nonlinear effects of co-located antennas.

From 1985 to 1987, he was an Engineering Technician at M/A COM Inc., where he was involved with the Controlled Components Group. In 1987, he joined the Haystack Observatory, Massachusetts Institute of Technology (MIT), Lexington, as a RF Technician supporting the Lincoln Laboratory's long range imaging radar (LRIR) system. In 1993, he became a Technical Staff Member involved with the development of low-noise receivers and frequency-generation systems for the Lincoln Laboratory's haystack auxiliary (HAX) radar. In 2000, he joined the Lincoln Laboratory as a Technical Staff Member in the Electro-Optic Materials and Devices Group, where he is currently involved in the development of ADCs utilizing optical sampling techniques. His research interests include phase noise characteristics of RF and optical devices, integration of optical sampling techniques into radar systems, low-noise RF sources, and nonlinear effects of receiver systems.

Mr. Hargreaves is a member of the IEEE Lasers and Electro-Optics Society (IEEE LEOS) and Sigma Xi.

Richard D. Younger was born in Denver, CO, in 1978. He received the B.S. degree in engineering physics (*magna cum laude*) from the University of Colorado at Boulder, in 2000.

His research accomplishments at the University of Colorado at Boulder include the development of a desktop demonstration of a strongly bound charged plasma at the Center for Integrated Plasma Studies and a theoretical investigation of electron transport in quantum heterostructures at the Joint Institute for Laboratory Astrophysics (JILA). He is currently an Assistant Technical Staff member at the Lincoln Laboratory, Massachusetts Institute of Technology, Lexington, where he is involved with the development of photonic ADCs.

Mr. Younger was a corecipient of the INFORMS Prize of the 2000 International Mathematical Contest in Modeling.

Jeffrey L. Wasserman (M'98) was born in Freehold, NJ, in 1975. He received the B.A. degree in physics from the University of Pennsylvania, Philadelphia, in 1997, and is currently working toward the Ph.D. degree in physics and The Johns Hopkins University, Baltimore, MD.

He was an Undergraduate Research Assistant while at the University of Pennsylvania, where he was a member of the High Energy Physics (HEP) Group, involved with the design and test low-noise charge detectors for use in international HEP experiments. In 1998, he joined the Electro-Optical Materials and Devices Group, Lincoln Laboratory, Massachusetts Institute of Technology, Lexington, where he was involved in the development of optically sampled ADCs.

Mr. Wasserman is a member of IEEE Lasers and Electro-Optics Society (IEEE LEOS), the Optical Society of America, and the Society of Physics Students. He was a recipient of the Swomley Fellowship for Graduate Physics at The Johns Hopkins University.

Fredrick J. O'Donnell, photograph and biography not available at time of publication.

Kevin G. Ray, photograph and biography not available at time of publication.

Richard C. Williamson (M'72–SM'80–F'82) received the B.S. and Ph.D. degrees in physics from the Massachusetts Institute of Technology (MIT), Cambridge, and in 1961 and 1966, respectively.

In 1970, he joined the Lincoln Laboratory, MIT, Lexington, where he is currently a Senior Staff Member in the Electro-Optical Materials and Devices Group. He has led research and development efforts on electrooptical materials and devices, including RF photonics, optical signal processing, optical modulators, semiconductor lasers, integrated optical circuits and microoptics.

Dr. Williamson is a member of the American Physical Society and the Optical Society of America. From 1980 to 1981, he was the National Lecturer of the IEEE Ultrasonics, Ferroelectrics, and Frequency Control Society. He is an associate editor for the IEEE PHOTONIC TECHNOLOGY LETTERS and the Program co-chair for the 2001 IEEE Lasers and Electro-Optics Conference. He was the recipient of the 1984 IEEE Centennial Medal and the 1985 Career Achievement Award from the IEEE for his work in ultrasonic physics, devices, and applications.